Novel Photocatalytic Function of Porphyrin-Modified Gold Nanoclusters in Comparison with the Reference Porphyrin Compound

Shunichi Fukuzumi,*,† Yoshiyuki Endo,† Yukiyasu Kashiwagi,† Yasuyuki Araki,‡ Osamu Ito,*,‡ and Hiroshi Imahori*,§,#

Department of Material and Life Science, Graduate School of Engineering, Osaka University, CREST, Japan Science and Technology Corporation (JST), Suita, Osaka 565-0871, Japan, Institute of Multidisciplinary Research for Advanced Materials, Tohoku University, CREST, JST, Katahira, Aoba-ku, Sendai 980-8577, Japan, Department of Molecular Engineering, Graduate School of Engineering, Kyoto University, PRESTO, JST, Sakyo-ku, Kyoto 606-8501, Japan, and Fukui Institute for Fundamental Chemistry, Kyoto University, 34-4, Takano-Nishihiraki-cho, Sakyo-ku, Kyoto 606-8103, Japan

Received: June 3, 2003

The photocatalytic function of three-dimensional porphyrin monolayer-protected gold clusters (MPCs) with different chain lengths has been examined in photocatalytic reduction of hexyl viologen (HV^{2+}) by 1-benzyl-1,4-dihydronicotinamide (BNAH) in comparison with that of the reference porphyrin compound without metal clusters. Both porphyrin monolayer-protected gold clusters and the reference porphyrin compound act as efficient photocatalysts for the uphill reduction of HV^{2+} by BNAH to produce 1-benzylnicotinamidinium ion (BNA^+) and hexyl viologen radical cation ($HV^{\bullet+}$) in benzonitrile. In the case of porphyrin monolayer-protected gold clusters the quantum yield reaches a maximum value with an extremely low concentration of HV^{2+}, which is larger than the corresponding value of the reference porphyrin compound. The dependence of quantum yields on concentrations of BNAH and HV^{2+} as well as the time-resolved single-photon-counting fluorescence and transient absorption spectroscopic results indicates that the photoinduced electron transfer from the triplet excited state of the reference porphyrin to HV^{2+} initiates the photocatalytic reduction of HV^{2+} by BNAH, but that the photoinduced electron transfer from the singlet excited state of porphyrin monolayer-protected gold clusters to HV^{2+}, which forms complexes with MPCs, is responsible for the photocatalytic reaction. The intersystem crossing from the porphyrin singlet excited state to the triplet is much suppressed by the quenching of the porphyrin excited singlet state via energy transfer to the gold surface of the three-dimensional MPCs. However, the three-dimensional architectures of porphyrin MPCs with large surface areas allow HV^{2+} to interact with MPCs, resulting in fast electron transfer from the singlet excited state of porphyrin to HV^{2+} on MPCs. This is the reason the quantum yield of the photocatalytic reduction of HV^{2+} by BNAH reaches a maximum value at an extremely small concentration of HV^{2+} when the surface of MPCs is covered by HV^{2+}. The light-harvesting efficiency of MPCs is much improved as compared with the reference compound.

Introduction

The preparation and properties of narrowly distributed nanoscopic metal colloids or metal nanoclusters have been intensively studied because of the anticipation of various applications of the unique electronic, optic, magnetic, and catalytic functions that bring new perspectives in science and technology.[1−10] On the other hand, self-assembled monolayers (SAMs) of organic molecules on flat metal surfaces have offered an excellent environment for molecular recognition by densely packed, highly ordered structures of organic molecules.[11−13] In particular, self-assembly of porphyrins bearing molecular recognition units on flat metal surfaces has attracted considerable attention because of the convenient preparation and the variety of applications including photovoltaic devices.[11−14] In contrast to SAMs on flat metal surfaces, organic monolayers on metal nanoclusters, so-called monolayer-protected metal clusters (MPCs), have provided three-dimensional (3D) materials, the putative parallels to the planar metal surfaces.[15−21] MPCs are stable in air and soluble in both nonpolar and polar organic solvents, thereby being capable of facile modification with a number of functional thiols through exchange reactions or by couplings and nucleophilic substitutions.[15−21] Construction of such 3D architectures of porphyrin MPCs that have large surface areas has improved the light-harvesting efficiency as compared to the 2D porphyrin SAMs.[22] In addition, the interaction of porphyrin excited states with gold nanoclusters is reduced significantly, relative to bulk gold surface, due to the "quantum effect",[23,24] enabling the development of a new type of light-harvesting materials.[22] Despite the extensive use of metal nanoclusters as photocatalysts,[6,25] the photocatalytic function of MPCs has yet to be scrutinized.[26]

We report herein the photocatalytic function of three-dimensional porphyrin monolayer-protected gold clusters (MPCs) with different chain lengths in photocatalytic reduction of hexyl viologen (HV^{2+}) by 1-benzyl-1,4-dihydronicotinamide (BNAH) in comparison with that of the reference porphyrin compound without metal clusters. Determination of quantum yields and

* Corresponding authors. E-mail: fukuzumi@ap.chem.eng.osaka-u.ac.jp; ito@tagen.tohoku.ac.jp; imahori@scl.kyoto-u.ac.jp.
† Osaka University, CREST.
‡ Tohoku University, CREST.
§ Kyoto University, PRESTO.
# Fukui Institute for Fundamental Chemistry, Kyoto University.

10.1021/jp0355509 CCC: $25.00
Published on Web 10/07/2003

the measurements of the time-resolved single-photon-counting fluorescence and transient absorption spectra of the photocatalytic system provide valuable insight into the novel photocatalytic mechanism of MPCs.

Experimental Section

Materials. The porphyrin-modified gold nanoclusters [H_2-PCnAuMPC ($n = 3, 11$)] were directly prepared by reduction of $HAuCl_4$ with $NaBH_4$ in toluene/water containing the porphyrin alkanethiol ($HAuCl_4$ = 1:1) to increase the extent of functionalization as reported previously.[22] To increase the solubility and reduce self-quenching of the porphyrin excited state, bulky *tert*-butyl substituents were introduced into *meta*-positions of the *meso*-phenyl ring on the porphyrin core. The characterization of porphyrin-modified nanoclusters (H_2-PCnAuMPC [$n = 3, 11$]) has been reported elsewhere.[22] The reference porphyrin compound (H_2P-ref) was also prepared as reported previously.[14a] Preparation of 1-benzyl-1,4-dihydronicotinamide (BNAH) and *N*,*N*′-dihexyl-4,4′-dipyridinium diperchlorate (HV^{2+}) was described previously.[27] Tetrabutylammonium hexafluorophosphate used as a supporting electrolyte for the electrochemical measurements was obtained from Tokyo Kasei Organic Chemicals. Benzonitrile was purchased from Wako Pure Chemical Ind., Ltd. and purified by successive distillation over calcium hydride.[28]

Quantum Yield Determinations. A standard actinometer (potassium ferrioxalate)[29] was used for the quantum yield determination of the photochemical reactions of BNAH with hexyl viologen in the presence of H_2P-ref or H_2PCnAuMPC. Typically, a square quartz cuvette (10 mm i.d.) that contained a deaerated PhCN solution (3.0 cm^3) of H_2P-ref (2.0×10^{-6} M), BNAH (10 mM), and HV^{2+} (20 mM) was irradiated with monochromatized light of $\lambda = 422$ nm from a Shimadzu RF-5000 fluorescence spectrophotometer. Under the conditions of actinometry experiments, the actinometer and H_2P-ref absorbed essentially all the incident light of $\lambda = 422$ nm. The light intensity of monochromatized light of $\lambda = 422$ nm was determined as 8.64×10^{-9} einstein s^{-1} with a slit width of 5 nm. The photochemical reaction was monitored using a Hewlett-Packard 8452A diode array spectrophotometer. The quantum yields in the absence of oxygen were determined from the increase in absorbance due to $HV^{\bullet+}$ at 615 nm ($\epsilon = 10\,000$ M^{-1} cm^{-1}).[27] To avoid the contribution of light absorption of the products, only the initial rates were used for determination of the quantum yields.

Spectral Measurements. UV−visible spectra were obtained on a Shimadzu UV-3100PC spectrometer or a Hewlett-Packard 8452A diode array spectrophotometer at 298 K. Corrected fluorescence spectra were taken using a SPEX Fluorolog 2 spectrometer, a Perkin-Elmer LS50B fluorescence spectrophotometer, or a Shimadzu spectrofluorophotometer (RF-5000PC). The solutions were deaerated by argon purging for 7 min prior to the measurements. Fluorescence decay curves on gold surface and in solutions were measured by means of a time-correlated single-photon-counting method using the second harmonic (435 nm) of Ti:sapphire laser (Coherent MIRA 900).

Laser Flash Photolysis. Nanosecond transient absorption measurements were carried out using SHG (532 nm) of a Nd:YAG laser (Spectra-Physics, Quanta-Ray GCR-130, fwhm 6 ns) as an excitation source. For transient absorption spectra in the near-IR region (600−1600 nm), monitoring light from a pulsed Xe lamp was detected with a Ge-avalanche photodiode (Hamamatsu Photonics, B2834). Photoinduced electron transfer in micro- and millisecond time regions was monitored by using a continuous Xe lamp (150 W) and an InGaAs-PIN photodiode (Hamamatsu Photonics, G5125-10) as a probe light and a detector, respectively. Details of the transient absorption measurements were described elsewhere.[30] All the samples in a quartz cell (1 × 1 cm) were deaerated by bubbling argon through the solution for 15 min.

Electrochemical Measurements. Cyclic voltammetry measurements were performed at 298 K on a BAS 100W electrochemical analyzer or a BAS CV-50W voltammetric analyzer in deaerated PhCN containing 0.1 M *n*-Bu_4NPF_6 as a supporting electrolyte at 298 K. A conventional three-electrode cell was used with a platinum working electrode and a platinum wire as a counter electrode. The measured potentials were recorded with respect to $Ag/AgNO_3$ (1.0×10^{-2} M). The E^0_{ox} and E^0_{red} values (vs Ag/Ag^+) are converted to those vs SCE by adding 0.29 V, respectively.[31]

Results and Discussion

Redox Properties of Porphyrin-Modified Au Nanoclusters. The structures of porphyrin-modified Au nanoclusters (H_2-PCnAuMPC, $n = 3, 11$) and the reference porphyrin compound (H_2P-ref) employed as photocatalysts in this study are shown in Chart 1, and they are fully characterized as reported elsewhere.[22] Narrowly distributed nanoscopic metal clusters are obtained as indicated by the mean diameters of the gold core, which were determined by transmission electron microscopy (TEM): $2R_{CORE} = 2.1$ nm (with a standard deviation $\sigma = 0.3$ nm) for H_2PC_{11}AuMPC and $2R_{CORE} = 2.0$ nm ($\sigma = 0.5$ nm) for H_2PC3AuMPC.[22]

The one-electron redox potentials of H_2PCnAuMPC and H_2P-ref, which are important properties for photoredox reactions, are determined by cyclic voltammetry as shown in Figure 1. The one-electron oxidation and reduction potentials (E^0_{ox} and E^0_{red} vs SCE) of H_2PC11AuMPC in benzonitrile (PhCN) are obtained as 0.94 and −1.22 V, respectively. The same values are obtained for the reference compound (H_2P-ref) as listed in Table 1. Thus, the interaction between the porphyrin and gold nanoparticles does not affect the redox potential of the porphyrin. The one-electron oxidation and reduction potentials of the singlet and triplet excited states ($^1E^0_{ox}{}^*$, $^3E^0_{ox}{}^*$, $^1E^0_{red}{}^*$, $^3E^0_{red}{}^*$) are determined by subtracting and adding the singlet and triplet excitation energies from the redox potentials of the ground states, and they are also listed in Table 1.

Photocatalytic Reduction of HV^{2+} by BNAH. The photocatalytic reaction examined in this study is the one-electron reduction of HV^{2+} by BNAH to produce 2 equiv of the one-electron-reduced species ($HV^{\bullet+}$) and 1 equiv of the two-electron-oxidized species (BNA^+) as shown in eq 1. The free energy

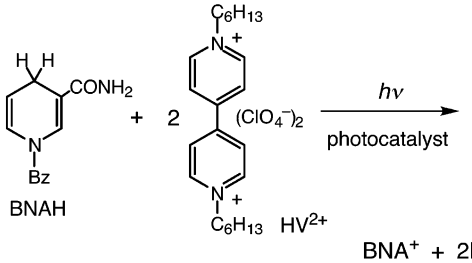

$$BNA^+ + 2HV^{\bullet+} + H^+ \quad (1)$$

change of the reaction (ΔG) is determined as 0.88 eV (85 kJ mol^{-1}) based on the difference between the redox potentials of BNAH/BNA^+ (0.02 V vs SCE)[32] and $HV^{2+}/HV^{\bullet+}$ (−0.42 V vs SCE)[27] in PhCN using eq 2. Because of the endergonic nature

$$\Delta G = 2F[E^0(\mathrm{BNAH/BNA^+}) - E^0(\mathrm{HV^{2+}/HV^{\bullet+}})] \quad (2)$$

of the reaction ($\Delta G > 0$), no reaction takes place thermally.

CHART 1

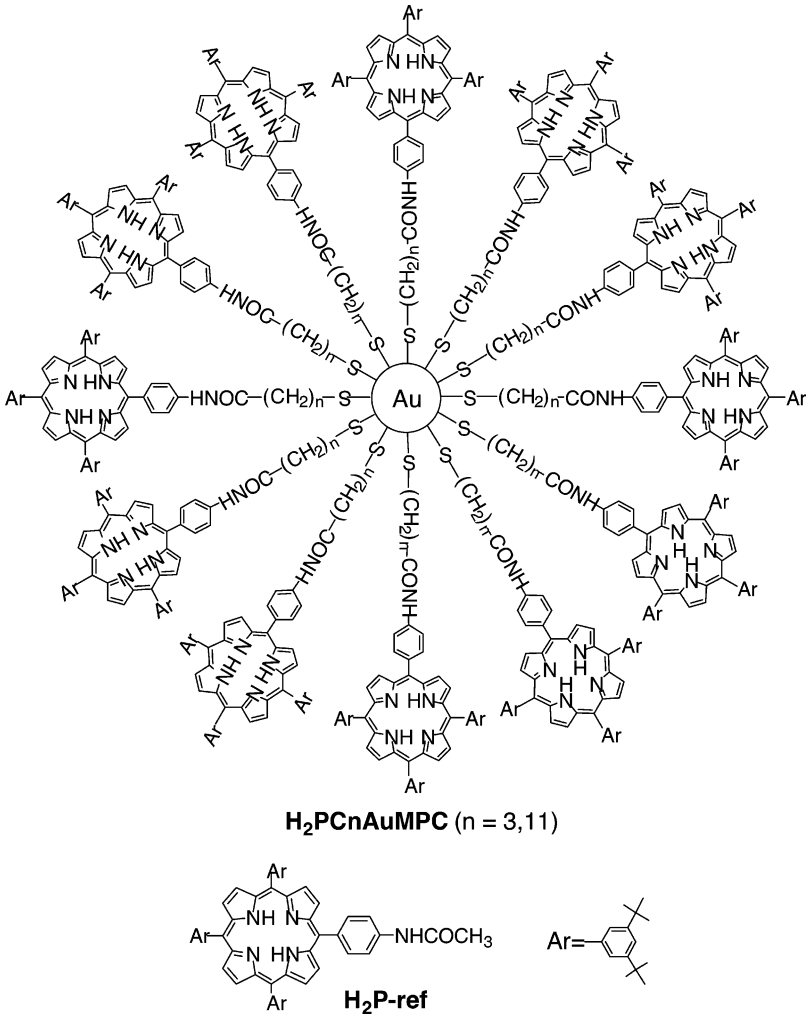

TABLE 1. Energies and Redox Potentials in H_2PC11AuMPC and H_2P-ref

	energy		redox potential					
compound	singlet excited state (eV)	triplet excited state (eV)	E^0_{red} (V)	E^0_{ox} (V)	$^1E^0_{red}{}^*$ (V)	$^1E^0_{ox}{}^*$ (V)	$^3E^0_{red}{}^*$ (V)	$^3E^0_{ox}{}^*$ (V)
H_2PC11AuMPC	1.91	1.40	−1.22	0.94	0.69	−0.97	0.18	−0.46
H_2P-ref	1.91	1.40	−1.22	0.94	0.69	−0.97	0.18	−0.46

However, addition of H_2PC11AuMPC as a photocatalyst to the BNAH/HV^{2+} system and photoirradiation of the Soret band (422 nm) result in the one-electron reduction of HV^{2+} as shown in Figure 2, where the absorption bands (λ_{max} = 402 and 615 nm) due to $HV^{\bullet+}$ increase progressively with irradiation time. The produced $HV^{\bullet+}$ is stable in deaerated PhCN. Similarly the photocatalytic reduction of HV^{2+} by BNAH occurs in the presence of H_2PC3AuMPC or H_2P-ref.

The quantum yields (Φ_{obs}) for the photocatalytic reduction of HV^{2+} by BNAH in the presence of H_2PC11AuMPC, H_2-PC3AuMPC, or H_2P-ref were determined using a ferrioxalate actinometer[29] under irradiation with monochromatic light of λ = 422 nm. The results are summarized in Table 2. The dependence of Φ_{obs} on [HV^{2+}] is shown in Figure 3a. The Φ_{obs} value in the presence of H_2PC11AuMPC (2.0×10^{-6} M) is rather independent of HV^{2+} concentration, and the Φ_{obs} value (0.07) is not much decreased even at 1.0×10^{-5} M as compared with the value at 2.0×10^{-2} M (Φ_{obs} = 0.19) as shown in Figure 3b. In contrast, the Φ_{obs} value in the presence of H_2P-ref increases with increasing [HV^{2+}] to approach a constant value and further increases with increasing [HV^{2+}]. It should be noted that the Φ_{obs} values of H_2PC11AuMPC are larger than the Φ_{obs} values of the reference compound (H_2P-ref) at low concentrations of HV^{2+} ($<1.0 \times 10^{-4}$ M) but that the order becomes opposite at higher concentrations. At each HV^{2+} concentration, the Φ_{obs} values of H_2PC11AuMPC are always larger than the Φ_{obs} values of H_2PC3AuMPC. In any case, the Φ_{obs} values are independent of BNAH concentrations at a fixed HV^{2+} concentration (Table 2). Thus, the dependence of Φ_{obs} on [HV^{2+}] is quite different between H_2PC11AuMPC and the reference compound (H_2P-ref). Such a difference indicates that the mechanism of the photocatalytic reaction is different between the porphyrin-modified nanocluster and the reference compound. The mechanistic difference is clarified from the laser flash photolysis experiments (vide infra).

Transient Absorption Spectra. The decay of the triplet excited state of H_2P-ref is monitored at 460 nm in the presence of BNAH or HV^{2+}. The decay rate was not affected by the presence of BNAH. The triplet lifetime is determined as 45 μs. In contrast, the addition of HV^{2+} results in the acceleration of

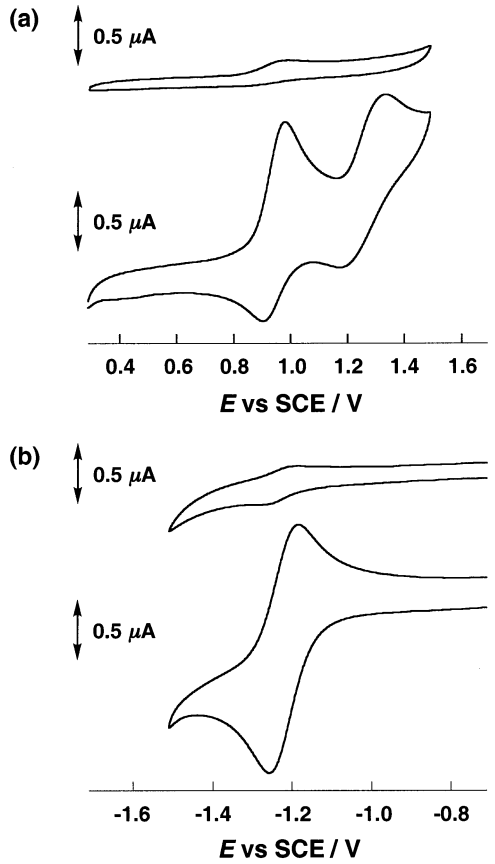

Figure 1. Cyclic voltammograms of $H_2PC11AuMPC$ (1.0×10^{-4} M based on the number of the porphyrins) and H_2P-ref (1.0×10^{-4} M) in PhCN solution containing 0.1 M *n*-Bu_4NPF_6 with a sweep rate of 0.01 V s^{-1}, platinum working electrode, platinum wire counter electrode, and $Ag/AgNO_3$ (1.0×10^{-2} M) reference electrode. (a) Oxidation of $H_2PC11AuMPC$ (top) and H_2P-ref (bottom) and (b) reduction of H_2-PC11AuMPC (top) and H_2P-ref (bottom).

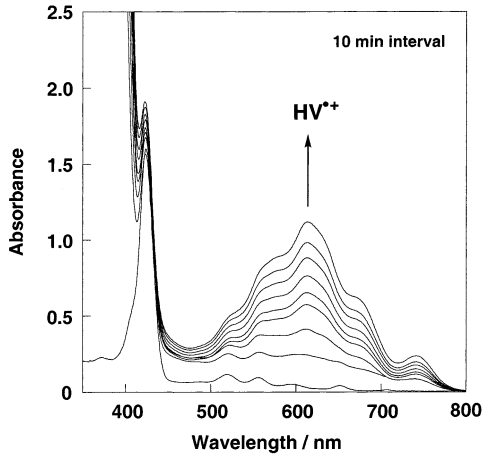

Figure 2. Spectral change observed in the steady-state photolysis of a PhCN solution of BNAH (10 mM), HV^{2+} (20 mM), and H_2-PC11AuMPC (1.6×10^{-6} M based on the number of the porphyrins) under irradiation of monochromatized light of $\lambda = 422$ nm.

decay of the triplet−triplet absorption at 460 nm, accompanied by the appearance of new absorption bands at 600 nm due to $HV^{\bullet+}$ and at 640 nm due to $H_2P^{\bullet+}$, as shown in Figure 4. The decay of the triplet−triplet absorption at 460 nm coincides with the appearance of the absorption at 600 nm due to $HV^{\bullet+}$ (Figure 5a). This indicates that electron transfer from the triplet excited state ($^3H_2P^*$) to HV^{2+} occurs to produce $H_2P^{\bullet+}$ and $HV^{\bullet+}$. The first-order decay rate constant of $^3H_2P^*$ increases linearly with

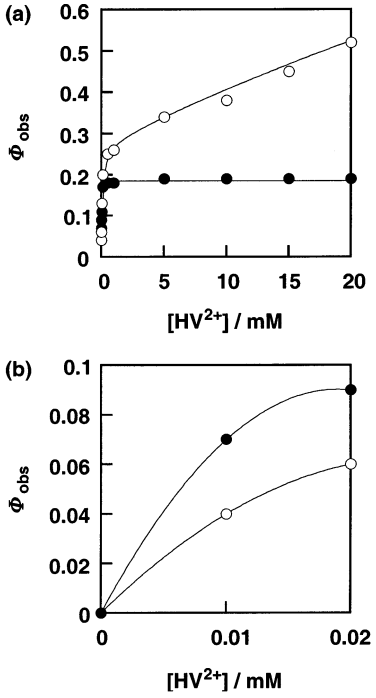

Figure 3. Quantum yields (Φ_{obs}) of photocatalytic reduction of HV^{2+} by BNAH (1.0×10^{-2} M) in the presence of (●) $H_2PC11AuMPC$ (2×10^{-6} M) or (○) H_2P-ref (2×10^{-6} M) in deoxygenated PhCN. The figures are shown in the range of (a) $[HV^{2+}] = (0-2) \times 10^{-2}$ M and (b) $[HV^{2+}] = (0-2) \times 10^{-5}$ M.

TABLE 2. Quantum Yields (Φ_{obs}) of Photocatalytic Reduction of HV^{2+} by BNAH (10 mM) in the Presence of Por-ref (2.0×10^{-6} M), $H_2PC11AuMPC$, or $H_2PC3AuMPC$ (2.0×10^{-6} M Based on the Number of the Porphyrins) in Deoxygenated PhCN

$[HV^{2+}]$/mM	Φ_{obs} (Por-ref)	Φ_{obs} ($H_2PC11AuMPC$)	Φ_{obs} ($H_2PC3AuMPC$)
1.0×10^{-2}	0.04	0.07	
2.0×10^{-2}	0.06	0.09	
5.0×10^{-2}	0.13	0.11	
1.0×10^{-1}	0.20	0.17	0.02
5.0×10^{-1}	0.25	0.18	0.02
1.0	0.26	0.18	0.03
5.0	0.34	0.19	0.04
10	0.38	0.19	0.06
15	0.45	0.19	0.08
20	0.52	0.19	0.10

increasing concentration of HV^{2+} (Figure 5b). From the slope of the linear plot in Figure 5b the second-order rate constant of electron transfer from $^3H_2P^*$ to HV^{2+} is determined as 2.4×10^8 M^{-1} s^{-1}. The free energy change of electron transfer from BNAH (E^0_{ox} vs SCE = 0.57 V)[33] to $^3H_2P^*$ (E^0_{red} vs SCE = 0.18 V) is positive ($\Delta G^0_{et} = 0.39$ eV), whereas the ΔG^0_{et} value of electron transfer from $^3H_2P^*$ (E^0_{ox} vs SCE = −0.46 V) to HV^{2+} (E^0_{red} vs SCE = −0.42 V)[26] is negative (−0.04 eV). Thus, electron transfer from BNAH to $^3H_2P^*$ is thermodynamically unfavorable, but electron transfer from $^3H_2P^*$ to HV^{2+} is expected to occur efficiently. This is consistent with the experimental observation (vide supra).

Photocatalytic Mechanism of H_2P-ref. The photocatalytic reduction of HV^{2+} by BNAH is started by photoinduced electron transfer from $^3H_2P^*$ to HV^{2+} rather than electron transfer from BNAH to $^3H_2P^*$, as shown in Scheme 1. At larger concentrations of HV^{2+}, photoinduced electron transfer from $^1H_2P^*$ to HV^{2+} may occur to produce $H_2P^{\bullet+}$ and $HV^{\bullet+}$. Since the one-electron reduction potential of $H_2P^{\bullet+}$, which is equivalent to the one-

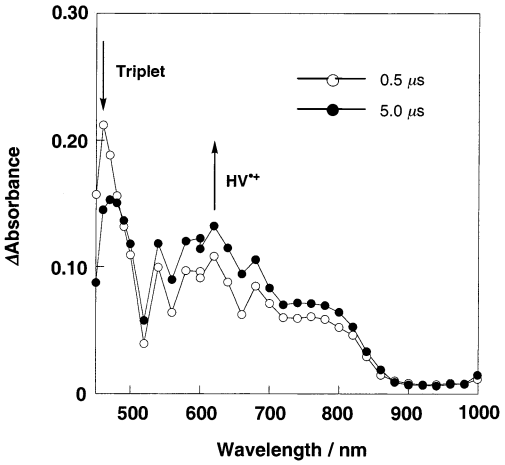

Figure 4. Nanosecond time-resolved transient absorption spectra of a PhCN solution containing H_2P-ref (2×10^{-6} M) and HV^{2+} (5×10^{-3} M) excited at 550 nm after laser irradiation (0.5 and 5.0 μs) in deaerated PhCN.

SCHEME 1

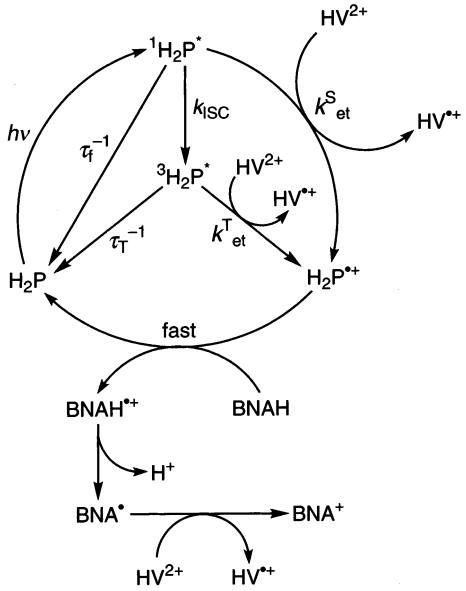

electron oxidation potential of H_2P (0.94 V), is more positive than the E^0_{ox} value of BNAH (0.57 V),[33] electron transfer from BNAH to $H_2P^{\bullet+}$ occurs efficiently to produce $BNAH^{\bullet+}$ accompanied by regeneration of H_2P. The deprotonation of BNAH is known to occur rapidly to produce $BNA^{\bullet}$.[33,34] Since $BNA^{\bullet}$ is a much stronger reductant than BNAH, electron transfer from $BNA^{\bullet}$ (E^0_{ox} vs SCE $= -1.08$ V)[33] to HV^{2+} ($E^0_{red} = -0.42$ V)[27] should occur efficiently to produce BNA^+ and $HV^{\bullet+}$.

By applying the steady-state approximation to the concentrations of $^1H_2P^*$, $^3H_2P^*$, and $H_2P^{\bullet+}$ in Scheme 1, the dependence of Φ_{obs} on $[HV^{2+}]$ can be derived as given by eq 3 (for the derivation, see Supporting Information):

$$\Phi_{obs} = \frac{2\,k_{ISC}\tau_f k^T_{et}\tau_T[HV^{2+}]}{(1 + k_{ISC}\tau_f + k^S_{et}\tau_f[HV^{2+}])(1 + k^T_{et}\tau_T[HV^{2+}])} + \frac{2k^S_{et}\tau_f[HV^{2+}]}{1 + k_{ISC}\tau_f + k^S_{et}\tau_f[HV^{2+}]} \quad (3)$$

where k_{ISC} is the rate constant of intersystem crossing from the singlet excited state to the triplet excited state, k^S_{et} is the rate

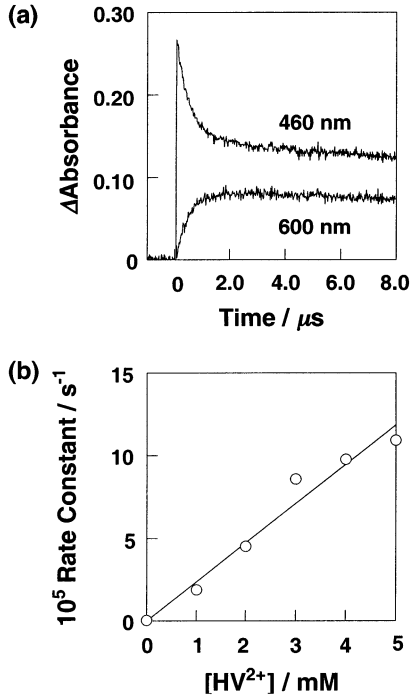

Figure 5. (a) Absorption−time profiles at 460 and 600 nm in a PhCN solution containing HV^{2+} (5×10^{-3} M) and H_2P-ref (2×10^{-6} M) and (b) plot of decay rate (first-order decay) vs $[HV^{2+}]$ for the photoinduced reduction of HV^{2+} by H_2P-ref (2×10^{-6} M).

constant of electron transfer from $^1H_2P^*$ to HV^{2+}, τ_f is the fluorescence lifetime of $^1H_2P^*$, k^T_{et} is the rate constant of electron transfer from $^3H_2P^*$ to HV^{2+}, and τ_T is the triplet lifetime of $^3H_2P^*$. The first term in eq 3 corresponds to the quantum yield from the triplet excited state, and the second term corresponds to the quantum yield from the singlet excited state. An increase in the Φ_{obs} value at low HV^{2+} concentration to reach a constant value corresponds to that from the triplet excited state (the first term in eq 3), and the further gradual increase in the Φ_{obs} value with concentration of HV^{2+} corresponds to the contribution from the singlet excited state (the second term in eq 3).

At low concentrations of HV^{2+} (<1 mM), the triplet pathway becomes dominant when $\Phi_{obs(T)}$ is given by eq 4. The $k^T_{et}\tau_T$

$$\Phi_{obs(T)} = \frac{2k_{ISC}\tau_f k^T_{et}\tau_T[HV^{2+}]}{(1 + k_{ISC}\tau_f)(1 + k^T_{et}\tau_T[HV^{2+}])} \quad (4)$$

value was determined as 1.1×10^4 M^{-1} from the k^T_{et} value (2.4×10^8 M^{-1} s^{-1}) and τ_T value (45 μs) in Figure 5b. In such a case, eq 4 is reduced to eq 5, since $k^T_{et}\tau_T[HV^{2+}] \gg 1$, where

$$\Phi_{obs(T)} = \frac{2k^{ISC}\tau_f}{1 + k_{ISC}\tau_f} \quad (5)$$

$\Phi_{obs(T)}$ is independent of concentration of HV^{2+}. The $k_{ISC}\tau_f$ value is determined as 0.16 from the limiting value of $\Phi_{obs(T)}$ (0.27) in eq 5. Since the τ_f value is determined as 9.9 ns by the fluorescence lifetime measurement of H_2P-ref, the k_{ISC} value is obtained as 1.6×10^7 s^{-1}.[35] The best fit line to eq 3 in Figure 3a (open circles) with the above-mentioned $k_{ISC}\tau_f$ and $k^T_{et}\tau_T$ values affords the $k^S_{et}\tau_f$ value (10 M^{-1}). A similar $k^S_{et}\tau_f$ value (16 M^{-1}) was independently determined from the fluorescence quenching of H_2P-ref by HV^{2+}. Thus, the dependence of Φ_{obs} on $[HV^{2+}]$ of H_2P-ref in Figure 3b is well reproduced by eq 3

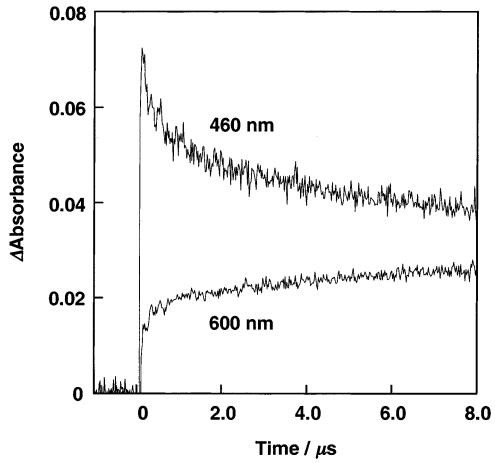

Figure 6. Absorption−time profiles at 460 and 600 nm in a PhCN solution containing HV^{2+} (5×10^{-3} M) and H_2PC11AuMPC (2×10^{-6} M).

using the rate constants and lifetimes determined independently. This confirms the validity of Scheme 1.

Photocatalytic Mechanism of H_2PC11AuMPC: Singlet Pathway. In contrast to the case of H_2P-ref, the decay of the triplet−triplet absorption of H_2PC11AuMPC does not coincide with the appearance of the absorption due to $HV^{\bullet+}$ at 600 nm as shown in Figure 6. There are three steps for formation of $HV^{\bullet+}$: the initial fast rise in the absorption, followed by the rapid and subsequent slow rise at 600 nm. The latter two steps coincide with the rapid and subsequent slow decay of the triplet−triplet absorption at 460 nm. The initial rapid formation of $HV^{\bullet+}$ may correspond to electron transfer from $^1H_2P^*$ to HV^{2+}. The $HV^{\bullet+}$ concentration formed in the initial fast step is constant irrespective of the concentration of HV^{2+} (Figure 7a). This indicates that an electron transfer from $^1H_2P^*$ to HV^{2+} occurs in the complex formed between H_2PC11AuMPC and HV^{2+}. Otherwise the $HV^{\bullet+}$ concentration would increase with increasing HV^{2+} concentration. The formation rate of $HV^{\bullet+}$ in the second step, which agrees with the decay rate of $^3H_2P^*$, is also constant irrespective of HV^{2+} concentration (Figure 7b). This indicates that electron transfer from $^3H_2P^*$ to HV^{2+} also occurs in the complex formed between H_2PC11AuMPC and HV^{2+}. The last slowest step corresponds to an intermolecular electron transfer from $^3H_2P^*$ to HV^{2+}. Judging from the ratio of the HV^{2+} concentration, which reaches a constant value in Figure 7 (1.0×10^{-3} M), to the porphyrin concentration in H_2-PC11AuMPC (2.0×10^{-6} M), only one HV^{2+} molecule is inserted into 500 porphyrin molecules. This also indicates that the interaction between HV^{2+} and porphyrins is relatively weak.

Similar results are obtained for H_2PC3AuMPC, as shown in Figure 8. In this case, the triplet−triplet absorption at 460 nm and the initial rise in absorption at 600 nm are significantly smaller than those in the case of H_2PC11AuMPC. This is consistent with the much shorter fluorescence lifetime (60 ps) of H_2PC3AuMPC due to the faster energy transfer from $^1H_2P^*$ to the gold nanocluster with the shorter chain length as compared with that of H_2PC11AuMPC (130 ps).

In contrast to the case of HV^{2+}, no fluorescence quenching of H_2PC11AuMPC occurs by BNAH even at 10 mM. The driving force for the complex formation between H_2PC11AuMPC and HV^{2+} may be the porphyrin−HV^{2+} $\pi-\pi$ stacking. Mizutani et al.[36] reported such porphyrin−guest $\pi-\pi$ stacking using gable-type porphyrins and DNA intercalators as hosts and guests, respectively. Porphyrin−guest $\pi-\pi$ stacking often induces a red-shift of the Soret band.[37] In the case of H_2PC11AuMPC,

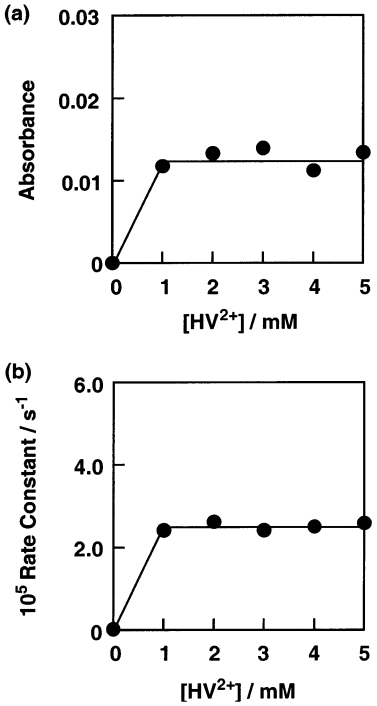

Figure 7. (a) Plot of absorbance (initial fast step at 600 nm) vs $[HV^{2+}]$ for photoinduced reduction of HV^{2+} by H_2PC11AuMPC (2×10^{-6} M) and (b) plot of decay rate (the second step at 600 nm) vs $[HV^{2+}]$ for photoinduced reduction of HV^{2+} by H_2PC11AuMPC (2×10^{-6} M).

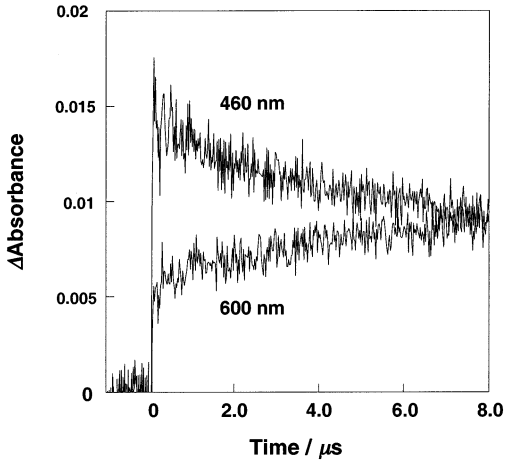

Figure 8. Absorption−time profiles at 460 and 600 nm in a PhCN solution containing HV^{2+} (5×10^{-3} M) and H_2PC3AuMPC (2×10^{-6} M).

however, no red-shift of the Soret band is observed in the presence of HV^{2+}; see Figure 2, where the Soret band (422 nm) of H_2PC11AuMPC in the presence of HV^{2+} is the same as that in the absence of HV^{2+} (422 nm). This indicates that the $\pi-\pi$ stacking is not strong enough to induce the red-shift of the Soret band. Despite the relatively weak binding between a porphyrin pair and HV^{2+}, large numbers of porphyrins attached on the gold nanoclusters may result in apparent strong binding between H_2PC11AuMPC and HV^{2+}.

The mechanism of the H_2PC11AuMPC-photocatalyzed reduction of HV^{2+} by BNAH is schematically summarized as shown in Scheme 2. In the presence of HV^{2+}, H_2PC11AuMPC binds HV^{2+} at small concentrations to form the complex H_2-PC11AuMPC/HV^{2+}. The photoexcitation of H_2PC11AuMPC/HV^{2+} results in formation of $^1H_2P^*$C11AuMPC/HV^{2+}, followed

SCHEME 2

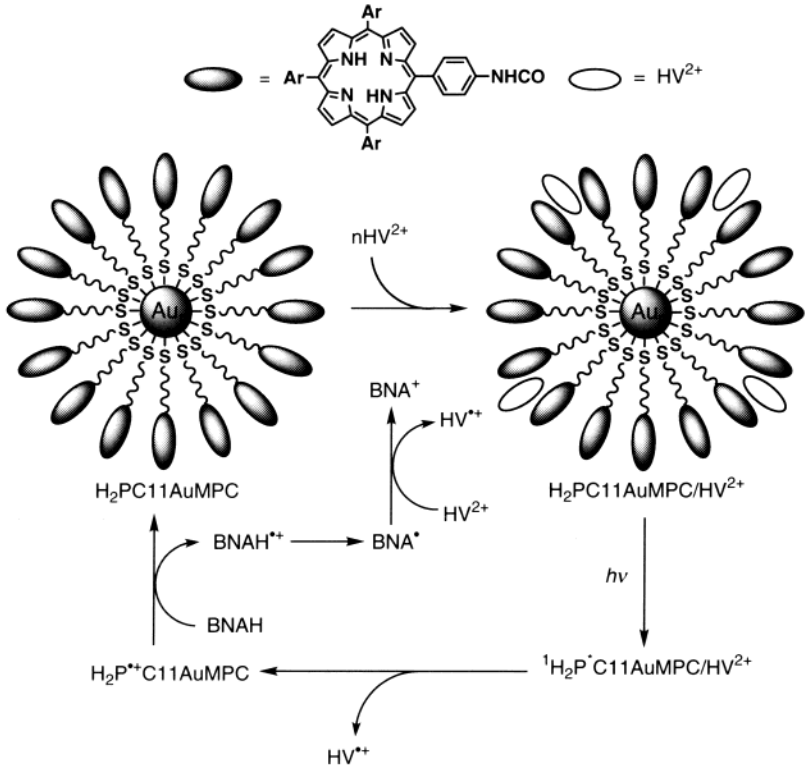

by efficient intracomplex photoinduced electron transfer from $^1H_2P^*$ to HV^{2+} to produce $H_2P^{\bullet+}$C11AuMPC and $HV^{\bullet+}$. The $H_2P^{\bullet+}$ moiety is reduced by BNAH to produce $BNAH^{\bullet+}$, accompanied by regeneration of H_2PC11AuMPC. The subsequent step is the same as the case of the reference porphyrin compound in Scheme 1: the deprotonation of $BNAH^{\bullet+}$, followed by electron transfer from $BNA^{\bullet}$ to HV^{2+}. In competition with the electron transfer from $^1H_2P^*$ to HV^{2+}, the intersystem crossing occurs to generate $^3H_2P^*$, which can also transfer an electron to HV^{2+} in $^3H_2P^*$C11AuMPC to produce $H_2P^{\bullet+}$C11AuMPC and $HV^{\bullet+}$. Judging from the results in Figure 7, the main reaction pathway is the intracomplex photoinduced electron transfer from $^1H_2P^*$ to HV^{2+}. This is the reason the quantum yield of $HV^{\bullet+}$ formation is rather constant irrespective of HV^{2+} concentration.

In contrast, the H_2P-ref-photocatalyzed reduction of HV^{2+} by BNAH occurs via an intermolecular photoinduced electron transfer from $^3H_2P^*$-ref to HV^{2+} (Scheme 1). Because of the mechanistic difference between the porphyrin-modified gold nanoclusters and the reference porphyrin compound, the porphyrin-modified gold nanoclusters act as a more efficient catalyst as compared with the reference porphyrin compound at low concentrations of HV^{2+} (Table 2). At high concentrations of HV^{2+}, however, no intermolecular photoinduced electron transfer from $^1H_2P^*$C11AuMPC to HV^{2+} takes place because of the short lifetime of the singlet excited state as compared to the reference porphyrin compound, resulting in smaller quantum yields than the reference system. The light-harvesting efficiency of the porphyrin-modified gold nanoclusters is certainly improved because of large porphyrin molecules contained on gold nanoclusters. Although the gold nanoclusters themselves have no direct photocatalytic function, the most important point of the use of the porphyrin-modified gold nanoclusters as photocatalysts is the binding function of a substrate (HV^{2+}), which enables the use of the singlet excited state for photoinduced electron transfer reactions at low substrate concentrations.

Acknowledgment. This work was partially supported by Grants-in-Aid for Scientific Research on Priority Areas (Nos. 11228205, 13440216) and a Grant-in-Aid for the Development of Innovative Technology (No. 12310) from the Ministry of Education, Culture, Sports, Science and Technology, Japan. H.I. thanks the Nagase Foundation for financial support.

Supporting Information Available: The derivation of eq 3 (S1). This material is available free of charge via the Internet at http://pubs.acs.org.

References and Notes

(1) (a) Schmid, G. *Chem. Rev.* **1992**, *92*, 1709. (b) Schmid, G. *Clusters and Colloids*; Wiley-VCH: Weinheim, 1994. (c) Schmid, G.; Bäumle, M.; Geerkens, M.; Helm, I.; Osemann, C.; Sawitowski, T. *Chem. Soc. Rev.* **1999**, *28*, 179.

(2) Lewis, L. N. *Chem. Rev.* **1993**, *93*, 2693.

(3) (a) Reetz, M. T.; Helbig, W.; Quaiser, S. A.; Stimming, U.; Breuer, N.; Vogel, R. *Science* **1995**, *267*, 367. (b) Aiken, J. D., III; Finke, R. G. *J. Am. Chem. Soc.* **1998**, *120*, 9545. (c) Bradley, J. S.; Tesche, B.; Busser, W.; Maase, M.; Reetz, M. T. *J. Am. Chem. Soc.* **2000**, *122*, 4631,

(4) (a) Chen, S. W.; Ingram, R. S.; Hostetler, M. J.; Pietron, J. J.; Murray, R. W.; Schaaff, T. G.; Khoury, J. T.; Alvarez, M. M.; Whetten, R. L. *Science* **1998**, *280*, 2098. (b) Elghanian, R.; Storhoff, J. J.; Mucic, R. C.; Letsinger, R. L.; Mirkin, C. A. *Science* **1997**, *277*, 1078. (c) Andres, R. P.; Bielefeld, J. D.; Henderson, J. I.; Janes, D. B.; Kolagunta, V. R.; Kubiak, C. P.; Mahoney, W. J.; Osifchin, R. G. *Science* **1996**, *273*, 1690. (d) Sun, S. H.; Murray, C. B.; Weller, D.; Folks, L.; Moser, A. *Science* **2000**, *287*, 1989.

(5) (a) Thathagar, M. B.; Beckers, J.; Rothenberg, G. *J. Am. Chem. Soc.* **2002**, *124*, 11858. (b) Kim, S.-W.; Kim, M.; Lee, W. Y.; Hyeon, T. *J. Am. Chem. Soc.* **2002**, *124*, 7642.

(6) (a) Duonghong, D.; Borgarello, E.; Grätzel, M. *J. Am. Chem. Soc.* **1981**, *103*, 4685. (b) Kurihara, K.; Kizling, J.; Stenius, P.; Fendler J. H. *J. Am. Chem. Soc.* **1983**, *105*, 2574. (c) Toshima, N.; Wang, Y. *Langmuir* **1994**, *10*, 4574. (d) Toshima, N. *Supramol. Sci.* **1998**, *5*, 395.

(7) (a) Ebitani, K.; Choi, K.-M.; Mizugaki, T.; Kaneda, K. *Langmuir* **2002**, *18*, 1849. (b) Ebitani, K.; Fujie, Y.; Kaneda, K. *Langnuir* **1999**, *15*, 3557.

(8) (a) Ghosh, S. K.; Kundu, S.; Mandal, M.; Pal, T. *Langmuir* **2002**, *18*, 8756. (b) Sau, T. K.; Pal, A.; Pal, T. *J. Phys. Chem. B* **2001**, *105*, 9266.

(9) (a) Haruta, M. *Catal. Today* **1997**, *36*, 153. (b) Kim, T. S.; Stiehl, J. D.; Reeves, C. T.; Meyer, R. J.; Mullins, C. B. *J. Am. Chem. Soc.* **2003**, *125*, 2018.

(10) (a) Finke, R. G. *Transition-Metal Nanoclusters: Solution-Phase Synthesis, then Characterization and Mechanism of Formation, of Polyoxoanion- and Tetrabutylammonium-Stabilized Nanoclusters.* In *Metal Nanoparticles: Synthesis, Characterization and Applications*; Feldheim, D. L., Foss, C. A., Jr., Eds.; Marcel Dekker: New York, 2002; Chapter 2, pp 17−54. (b) Özkar, S.; Finke, R. G. *J. Am. Chem. Soc.* **2002**, *124*, 5796.

(11) (a) Ulman, A. *Chem. Rev.* **1996**, *96*, 1533. (b) Willner, I.; Doron, A.; Katz, E. *J. Phys. Org. Chem.* **1998**, *11*, 546. (c) Lahav, M.; Gabriel, T.; Shipway, A. N.; Willner, I. *J. Am. Chem. Soc.* **1999**, *121*, 258. (d) Shipway, A. N.; Katz, E.; Willner, I. *ChemPhysChem* **2000**, *1*, 18.

(12) (a) Fukuzumi, S.; Imahori, H. In *Electron Transfer in Chemistry*; Balzani, V., Ed.; Wiley-VCH: Weinheim, 2001; Vol. 2, pp 927−975. (b) Imahori, H.; Sakata, Y. *Eur. J. Org. Chem.* **1999**, *2445*, 5. (c) Imahori, H.; Mori, Y.; Matano, Y. *J. Photochem. Photobiol. C* **2003**, *4*, 51.

(13) (a) Uosaki, K.; Kondo, T.; Zhang, X.-Q.; Yanagida, M. *J. Am. Chem. Soc.* **1997**, *119*, 8367. (b) Kondo, T.; Kanai, T.; Iso-o, K.; Uosaki, K. *Z. Phys. Chem.* **1999**, *212*, 23.

(14) (a) Imahori, H.; Norieda, H.; Nishimura, Y.; Yamazaki, I.; Higuchi, K.; Kato, N.; Motohiro, T.; Yamada, H.; Tamaki, K.; Arimura, M.; Sakata, Y. *J. Phys. Chem. B* **2000**, *104*, 1253. (b) Imahori, H.; Yamada, H.; Nishimura, Y.; Yamazaki, I.; Sakata, Y. *J. Phys. Chem. B* **2000**, *104*, 2099. (c) Imahori, H.; Norieda, H.; Yamada, H.; Nishimura Y.; Yamazaki, I.; Sakata, Y.; Fukuzumi, S. *J. Am. Chem. Soc.* **2001**, *123*, 100. (d) Yamada, H.; Imahori, H.; Nishimura, Y.; Yamazaki, I.; Fukuzumi, S. *J. Chem. Soc., Chem. Commun.* **2000**, 1921. (e) Yamada, H.; Imahori, H.; Nishimura, Y.; Yamazaki, I.; Fukuzumi, S. *Adv. Mater.* **2002**, *14*, 892.

(15) (a) Brust, M.; Walker, M.; Bethell, D.; Schiffrin, D. J.; Whyman, R. *J. Chem. Soc., Chem. Commun.* **1994**, 801. (b) Templeton, A. C.; Wuelfing, W. P.; Murray, R. W. *Acc. Chem. Res.* **2000**, *33*, 27.

(16) (a) Mirkin, C. A.; Letsinger, R. L.; Mucic, R. C.; Storhoff, J. J. *Nature* **1996**, *382*, 607. (b) Alivisatos, A. P.; Johnsson, K. P.; Peng, X. G.; Wilson, T. E.; Loweth, C. J.; Bruchez, M. P.; Schultz, P. G. *Nature* **1996**, *382*, 609. (c) Mucic, R. C.; Storhoff, J. J.; Mirkin, C. A.; Letsinger, R. L. *J. Am. Chem. Soc.* **1998**, *120*, 12674. (d) Storhoff, J. J.; Mirkin, C. A. *Chem. Rev.* **1999**, *99*, 1849.

(17) (a) Ingram, R. S.; Hostetler, M. J.; Murray, R. W. *J. Am. Chem. Soc.* **1997**, *119*, 9175. (b) Liu, J.; Mendoza, S.; Román, E.; Lynn, M. J.; Xu, R.; Kaifer, A. E. *J. Am. Chem. Soc.* **1999**, *121*, 4304. (c) Templeton, A. C.; Cliffel, D. E.; Murray, R. W. *J. Am. Chem. Soc.* **1999**, *121*, 7081. (d) Hicks, J. F.; Zamborini, F. P.; Osisek, A. J.; Murray, R. W. *J. Am. Chem. Soc.* **2001**, *123*, 7048.

(18) (a) Boal, A. K.; Ilhan, F.; DeRouchey, J. E.; Thurn-Albrecht, T.; Russell, T. P.; Rotello, V. M. *Nature* **2000**, *404*, 746. (b) McIntosh, C. M.; Esposito, E. A., III; Boal, A. K.; Simard, J. M.; Martin, C. T.; Rotello, V. M. *J. Am. Chem. Soc.* **2001**, *123*, 7626. (c) Evans, S. D.; Johnson, S. R.; Ringsdorf, H.; Williams, L. M.; Wolf, H. *Langmuir* **1998**, *14*, 6436. (d) Liu, J.; Mendoza, S.; Román, E.; Lynn, M. J.; Xu, R.; Kaifer, A. E. *J. Am. Chem. Soc.* **1999**, *121*, 4304.

(19) (a) Boal, A. K.; Rotello, V. M. *J. Am. Chem. Soc.* **1999**, *121*, 4914. (b) Boal, A. K.; Rotello, V. M. *J. Am. Chem. Soc.* **2000**, *122*, 734. (c) Frankamp, B. L.; Uzun, O.; Ilhan, F.; Boal, A. K.; Rotello, V. M. *J. Am. Chem. Soc.* **2002**, *124*, 892. (d) Boal, A. K.; Rotello, V. M. *J. Am. Chem. Soc.* **2002**, *124*, 5019. (e) Frankamp, B. L.; Boal, A. K.; Rotello, V. M. *J. Am. Chem. Soc.* **2002**, *124*, 15146.

(20) (a) Fujiwara, H.; Yanagida, S.; Kamat, P. V. *J. Phys. Chem. B* **1999**, *103*, 2589. (b) Thomas, K. G.; Kamat, P. V. *J. Am. Chem. Soc.* **2000**, *122*, 2655. (c) Sudeep, P. K.; Ipe, B. I.; Yhomas, G.; Gerorge, M. V.; Barazzouk, S.; Hotchandani, S.; Kamat, P. V. *Nano Lett.* **2002**, *2*, 29. (d) Ipe, B. I.; Thomas, K. G.; Barazzouk, S.; Hotchandani, S.; Kamat, P. V. *J. Phys. Chem. B* **2002**, *106*, 18. (e) Kamat, P. V.; Barazzouk, S.; Hotchandani, S. *Angew. Chem., Int. Ed.* **2002**, *41*, 2764.

(21) (a) Zhang, J.; Whitesell, J. K.; Fox, M. A. *Chem. Mater.* **2001**, *13*, 2323. (b) Hu, J.; Zhang, J.; Liu, F.; Kittredge, K.; Whitesell, J. K.; Fox, M. A. *J. Am. Chem. Soc.* **2001**, *123*, 1464.

(22) (a) Imahori, H.; Arimura, M.; Hanada, T.; Nishimura, Y.; Yamazaki, I.; Sakata, Y.; Fukuzumi, S. *J. Am. Chem. Soc.* **2001**, *123*, 335. (b) Imahori, H.; Fukuzumi, S. *Adv. Mater.* **2001**, *13*, 1197.

(23) (a) Alivisatos, A. P. *Science* **1996**, *271*, 933. (b) Bawendi, M. G.; Steigerwald, M. L.; Brus, L. E. *Annu. Rev. Phys. Chem.* **1990**, *41*, 477. (c) Wang, Y. In *Advances in Photochemistry*; Neckers, D. C., Volman, D. H., von Bünau, G., Eds.; Wiley-VCH: New York, 1995; pp 179−234.

(24) (a) Kamat, P. V. In *Semiconductor Nanoclusters−Physical, Chemical and Catalytic Aspects*; Kamat, P. V., Meisel, D., Eds.; Elsevier Science: Amsterdam, 1997; pp 237−259. (b) Kamat, P. V. *J. Phys. Chem. B* **2002**, *106*, 7729. (c) Henglein, A. *Ber. Bunsen-Ges. Phys. Chem.* **1995**, *99*, 903. (c) Pileni, M. P. *New J. Chem.* **1998**, 693. (d) Link, S.; El-Sayed, M. A. *J. Phys. Chem. B* **1999**, *103*, 4212.

(25) (a) Wilcoxon, J. P. *J. Phys. Chem. B* **2000**, *104*, 7334. (b) Korgel, B. A.; Monbouquette, H. G. *J. Phys. Chem. B* **1997**, *101*, 5010. (c) Thurston, T. R.; Wilcoxon, J. P. *J. Phys. Chem. B* **1999**, *103*, 11.

(26) For the noncatalytic photochemical reactions of MPCs, see: Kell, A. J.; Stringle, D. L. B.; Workentin, M. S. *Org. Lett.* **2000**, *2*, 3381.

(27) Fukuzumi, S.; Imahori, H.; Okamoto, K.; Yamada, H.; Fujitsuka, M.; Ito, O.; Guldi, D. M. *J. Phys. Chem. A* **2002**, *106*, 1903.

(28) Perrin, D. D.; Armarego, W. L. F.; Perrin, D. R. *Purification of Laboratory Chemicals*; Pergamon Press: Elmsford, 1988.

(29) Hatchard, C. G.; Parker, C. A. *Proc. R. Soc. London, Ser. A* **1956**, *235*, 518.

(30) Fujitsuka, M.; Watanabe, A.; Ito, O.; Yamamoto, K.; Funasaka, H. *J. Phys. Chem. A* **1997**, *101*, 7960.

(31) Mann, C. K.; Barnes, K. K. *Electrochemical Reactions in Nonaqueous Systems*; Mercel Dekker: New York, 1970.

(32) Anne, A.; Moiroux, J.; Saveant, J.-M. *J. Org. Chem.* **2000**, *65*, 7213.

(33) Fukuzumi, S.; Koumitsu, S.; Hironaka, K.; Tanaka, T. *J. Am. Chem. Soc.* **1987**, *109*, 305.

(34) Fukuzumi, S.; Inada, O.; Suenobu, T. *J. Am. Chem. Soc.* **2002**, *124*, 14538.

(35) The k_{ISC} value of H_2TPP has been reported as 6.8×10^7 s^{-1}, which is larger than the estimated k_{ISC} value of H_2P-ref; see: Toyama, N.; Asano-Someda, M.; Ichino, T.; Kaizu, Y. *J. Phys. Chem. A* **2000**, *104*, 4857. The possible contribution of back electron transfer from $HV^{\bullet+}$ to $BNAH^{\bullet+}$ in Scheme 2 may result in a decrease in the limiting $\Phi_{obs(T)}$ value, leading to the smaller k_{ISC} value.

(36) Mizutani, T.; Wada, K.; Kitagawa, S. *J. Am. Chem. Soc.* **2001**, *123*, 6459.

(37) (a) Schneider, H.-J.; Wang, M. *J. Org. Chem.* **1994**, *59*, 7464. (b) Sirish, M.; Schneider, H.-J. *J. Am. Chem. Soc.* **2000**, *122*, 5881.